nature physics

SUPPLEMENTARY INFORMATION

DOI: 10.1038/NPHYS1738

Coherent dynamics of macroscopically ordered electronic states through a symmetry-breaking transition - Supplementary Information (SI)

by Yusupov et al.

Methods

The experimental setup.

An amplified Ti:Sapphire laser system was used as a source, giving 50 fs, 400 nm or 800 nm pulses with a repetition rate of 250 kHz and energies up to 1 μJ The pulse train was split into three components which were then suitably delayed and attenuated relative to each other. The destruction (D) pulse beam was the most intense, with $\Phi = 100$ μJ/cm^2 (for $TbTe_3$ and 400 nm excitation) or $\Phi = 680$ μJ/cm^2 (for $TbTe_3$ and 800 nm excitation), while the pump and the probe beam fluences were typically 5-10 μJ/cm^2 and 0.1 μJ/cm^2, respectively obtained by focusing on the sample with a 100 mm f.l. lens. The pump and probe had orthogonal polarizations, and

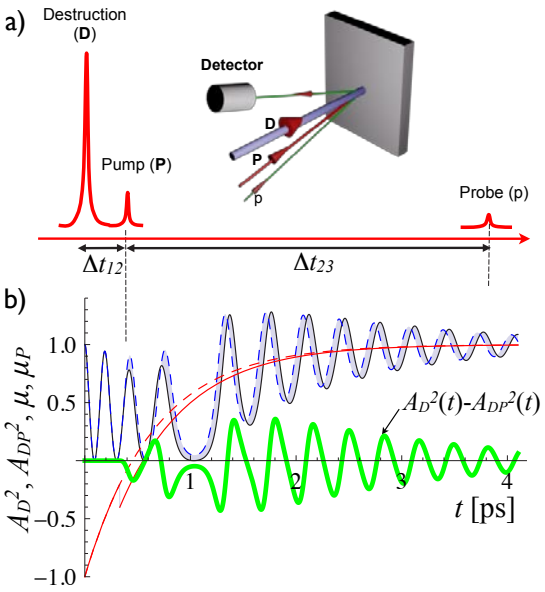

Figure 1: a) A schematic description of the experiment: The *destruction* (D) pulse quenches the system, while a *pump-probe* (P-p) sequence probes the reflectivity at a later time Δt_{12}. b) The control parameters μ (solid) and μ_P (dashed), with $\tau_{A_{sp}} = 0.65$ ps and $\triangle t_{12}$=0.4 ps. The predicted oscillations of $A^2(t)$ with, and without the P pulse are shown by the dashed and solid oscillatory curves respectively. The predicted $\Delta R(t)$ is shown by the green curve.

DOI: 10.1038/NPHYS1738

the angle of incidence was near-normal for all three beams. The response was recorded using homodyne detection with a variably delayed pump-probe(P-p) pulse sequence[1], so that we could monitor the re-appearance of QP and collective excitations by changing the time delay Δt_{12} between the *D* pulse and the *P* pulse (see Fig.1). The P pulse train was modulated at 2 kHz so the p pulses did not detect the signal from the D pulse. The single crystal growth is described in [2]. The samples were cleaved in a glove box prior to mounting into the cryostat, and the spot sizes were $\sim$ 80 μm in diameter for D and pump beams and $\sim$ 50 μm for the probe.

The system was kept at a base temperature of 15 K during the experiment, unless otherwise stated. The energy of the pulse was carefully adjusted so that it was just sufficient to destroy the ordered state.

The QP signal in Fig. 2a) is obtained by fitting a single (double in the case of $K_{0.3}MoO_3$) exponential decay with a finite exponential risetime. The risetime of $\Delta R/R$ is found to be independent of Δt_{12} and fluence.

Accurate determination of CDW state destruction threshold

To accurately identify the threshold where the CDW state is destroyed, we need to account for geometrical aspects due to the finite absorption length of pump and probe light as well as the transverse beam profiles [3]. In the probe beam, the sample penetration depth has to be accounted for twice (upon entering and exiting the sample). The relative photoinduced change in reflectivity is then given by:

$$\frac{\Delta R}{R} \propto \int_0^\infty \int_0^\infty \exp\left(-2\frac{z}{\lambda_{op}}\right)\exp\left(-\frac{r^2}{\rho_{pr}^2}\right) n_{qp}(r,z) r dr dz \tag{1}$$

where λ_{op} is optical penetration depth, and $2\rho_{pr}$ is probe beam diameter on the sample. We take the change of reflectivity to be linear with the density of photoexcited quasiparticles n_{qp}, and n_{qp} to be approximately linear with excitation density up to the threshold excitation fluence Φ_T where the CDW state is destroyed. For $\Phi > \Phi_T$ all quasiparticles are excited and n_{QP} saturates at n_s:

$$n_{qp} \approx \begin{cases} \frac{\Phi(r,z)}{\Phi_T} n_s & \Phi(r,z) < \Phi_T \\ n_s & \Phi(r,z) > \Phi_T \end{cases} . \tag{2}$$

The light fluence penetrating into the sample is $\Phi_0 = (1-R)\Phi_{pu}$ where Φ_{pu} represents the laser fluence on the surface of the sample. The laser fluence within the sample is:

$$\Phi(r,z) = \Phi_0 \exp\left(-\frac{z}{\lambda_{op}}\right)\exp\left(-\frac{r^2}{\rho_{pu}^2}\right) \tag{3}$$

Assuming that in the ungapped state $\Delta R/R$ does not depend on Φ due to other processes, we calculate the integral separately for $\Phi(r,z) < \Phi_T$ and $\Phi_T > \Phi_T$. With the pump beam radii ρ_{pu} and $\frac{1}{\rho_{eff}^2} = \left(\frac{1}{\rho_{pu}^2} + \frac{1}{\rho_{pr}^2}\right)$ the complete integral is:

$$\frac{\Phi_0}{\Phi_T} n_s \int_0^\infty \exp\left(-\frac{3z}{\lambda_{op}}\right)\left[\int_0^\infty \exp\left(\frac{-r^2}{\rho_{eff}^2}\right)\Theta\left(1-\frac{\Phi(r,z)}{\Phi_T}\right) r dr\right] dz$$

The CDW destruction threshold was thus accurately determined from the fit to be $47 \pm 2\mu$J/cm^2 for TbT_3 at 15 K. The destruction threshold was determined for all the other materials in the same way using experimental values of absorption depth λ and reflectivity R at the relevant wavelength (either 800 or 400 nm) in each case[4, 5, 6].

The optical response function.

To obtain the optical response, we can expand the dielectric constant near CDW phase transition in powers of the order parameter[7]:

$$\epsilon = \epsilon_0 + c_2|\Delta|^2 = \epsilon_0 + c_2 A^2. \tag{4}$$

DOI: 10.1038/NPHYS1738

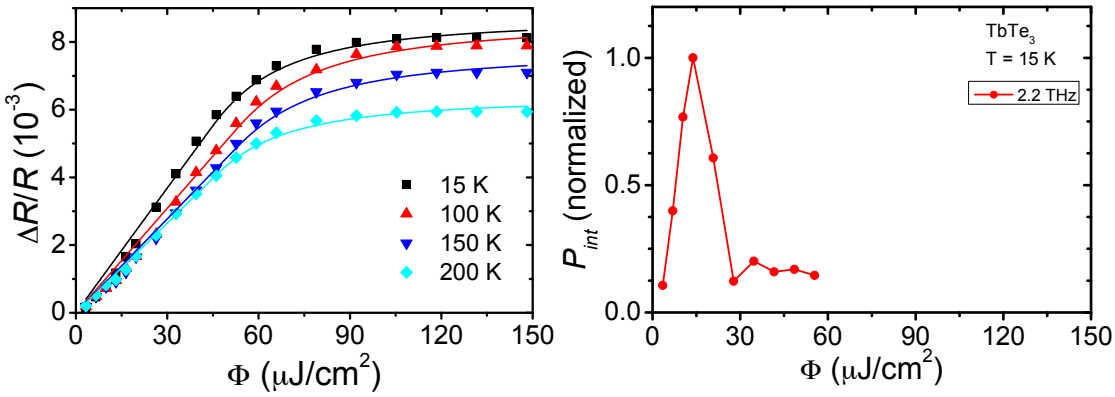

Figure 2: a) The amplitude of the photoinduced reflectivity as a function of fluence for 400 nm pump for $TbTe_3$. The lines are best fits of Eq. 1 to the data . b) The intensity of the AM P_{int} as a function of fluence Φ. The fluence refers to the value incident on the sample.

Here ϵ_0 is the dielectric constant of the high temperature symmetric phase, c_2 is a real constant. The transient reflectivity response function in the *P-p* experiment is given by the difference between the response *with* and *without* the pump P pulse:

$$\Delta R(t, \Delta t_{12}) = \left(\frac{\partial R}{\partial \epsilon}\right) \Delta\epsilon \propto \int [A^2_{DP}(t, \mathbf{r}, \Delta t_{12}) - A^2_D(t, \mathbf{r})] e^{-z/\lambda} d^3\mathbf{r}. \quad (5)$$

The integration takes into account the inhomogeneity arising from the finite optical penetration depth λ of the probe (*p*) pulses in the z direction, where $A^2_{DP}(t, z, \Delta t_{12})$ is calculated replacing η by $\eta_P(t) = \eta(0)\exp(-t/\tau_{sp}) + \Pi\Theta(t - t_{12})exp[-(t - t_{12})]/\tau_{sp})$. The exponential term accounts for the probe penetration depth. Π is the *P* pulse intensity relative to the *D* pulse and $\Theta(t - t_{12})$ is a unit step function. The typical experimental value of $\Pi = 0.1$.

For comparison, the more usual case discussed for coherent phonons assumes small oscillations of the order parameter near its equilibrium position, where we consider the amplitude mode: $Q = A - A_0$. Expanding the free energy in powers of Q:

$$F = F_0 - a^2(T - T_c)^2/2\beta + 2a(T_c - T)Q^2. \quad (6)$$

Here the second term in the right hand side of the equation describes the condensation energy and the last term describes the amplitude mode with frequency $\omega^2 \propto 2a(T_c - T)$, where a and β are positive parameters in the Ginzburg-Landau functional.

The detection of the amplitude mode through pump-probe experiments is determined by the dependence of the dielectric function on Q and has the following form, similar to that derived by Zeiger et al.[8]:

$$\epsilon = \epsilon_0 + c_2 A_0^2 + 2c_2 A_0 Q \quad (7)$$

As it is defined by Eq.(7) the nonzero order parameter brings the amplitude mode to $k = 0$. This

is possible because the wave-vector of the amplitude mode is compensated by the wave-vector of the order parameter.

Modelling the optical response arising from domain wall recombination.

In order to show that the observed distorted lineshapes in the ω-t plots (Fig. 3 of main text and Fig. 6 below) are not artifacts arising from inhomogeneous excitation intensity and/or depth dependence of mode parameters, we calculate and compare $\Psi(z,t)$ and the optical response (ω-t plots) for three limiting cases:

1. The homogeneous solution, where the medium is considered to be uniform as described by Eq. 2 of the main text, but without the spatial gradient term. (The parameters α, ω and η are experimentally determined and apply to $TbTe_3$, as given)

2. The inhomogeneous solution to Eq.2, where the z dependence of D, P and p pulses are all taken explicitly into account, as described in the main text. The parameters α, ω , $\lambda = 20$ nm, $\xi = 1.2$ nm and η = 2.2 are experimental and apply to $TbTe_3$.

3. An inhomogeneous solution to Eq.2, where the z dependence of D, P and p are all taken explicitly into account and the parameters α, ω and η are the same as in case (2) above, except for the coherence length ξ, which is changed to 0.8 nm. With these parameter values, no domain wall annihilation occurs on the relevant timescale, so no Ψ waves are emitted, and no resulting distortions in the spectro-temporal response are expected. (Note that we purposefully chosen this change of parameter ξ in such a way to obtain a solution with no annihilation events in the first 5 ps.)

The $A(z,t)$ and the optical response for three cases are shown in Figure 3. It is clear from the figures that only case (2), i.e. the inhomogeneous solution with domain wall annihilation displays the diagonal blobs in the $\omega - t$ spectra. These clearly arise when the field is distorted due to the undulations of Ψ emitted by the annihilation event reaching the surface. The homogeneous solution (case 1) without domain wall annihilation does *not* show this effect. The same is true for the inhomogeneous solution (case 3), in spite of the fact that the model specifically takes into account the excitation profile dependence on depth and the resulting frequency changes of the mode frequency with depth. Extensive and systematic calculations of $A(z,t)$ and the optical response within a wide parameter space of λ/ξ and $\eta(0)$ show that the features above are very robust. Here we have presented only the limiting cases, pertinent to the experimental situation.

Note that the shape of the spectral features in the $\omega - t_{12}$ plot obtained from the FFT of the temporal evolution of $A(z,t)$ are strongly weighted. The major part of the spectral weight comes from the oscillations well after t_c, (determined by the experimental value of the collective mode damping constant α). Since there are only a few waves at low frequency near the critical

DOI: 10.1038/NPHYS1738

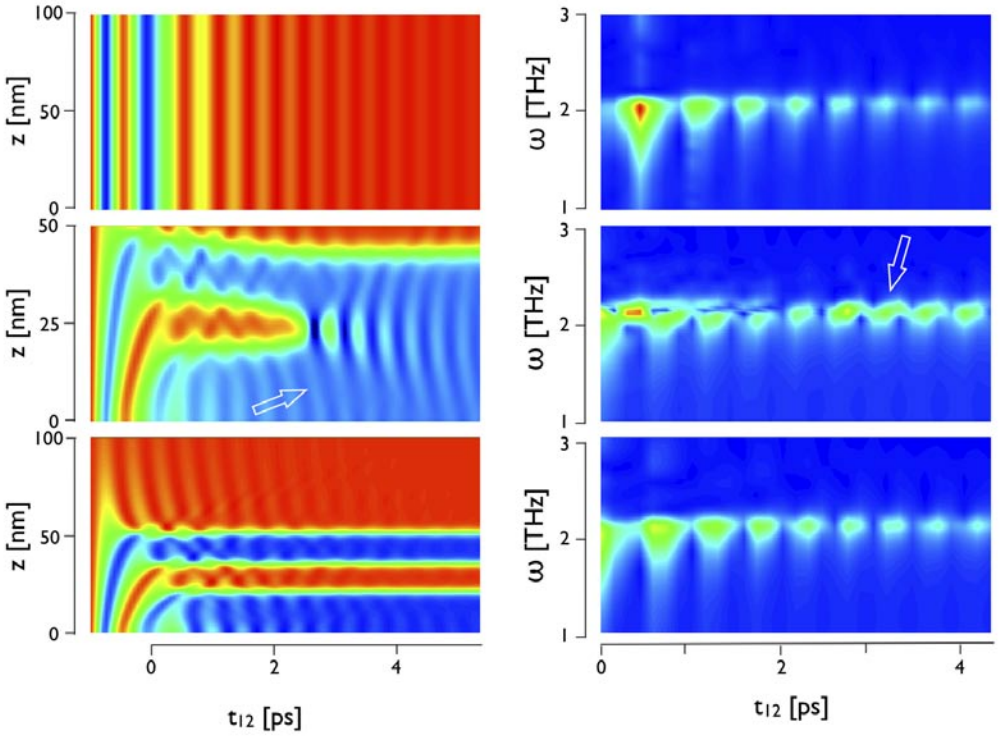

Figure 3: The order parameter Ψ (left column), and the optical spectral response (right column) as a function of time t_{12} after quench. The three cases (1)-(3) from top to bottom respectively correspond to the ones explained in the text. Arrows point to the A-waves. A 3D plot of case (2) is also shown in the main text (Fig. 4), where the A-waves are more clearly visible in the printed version.

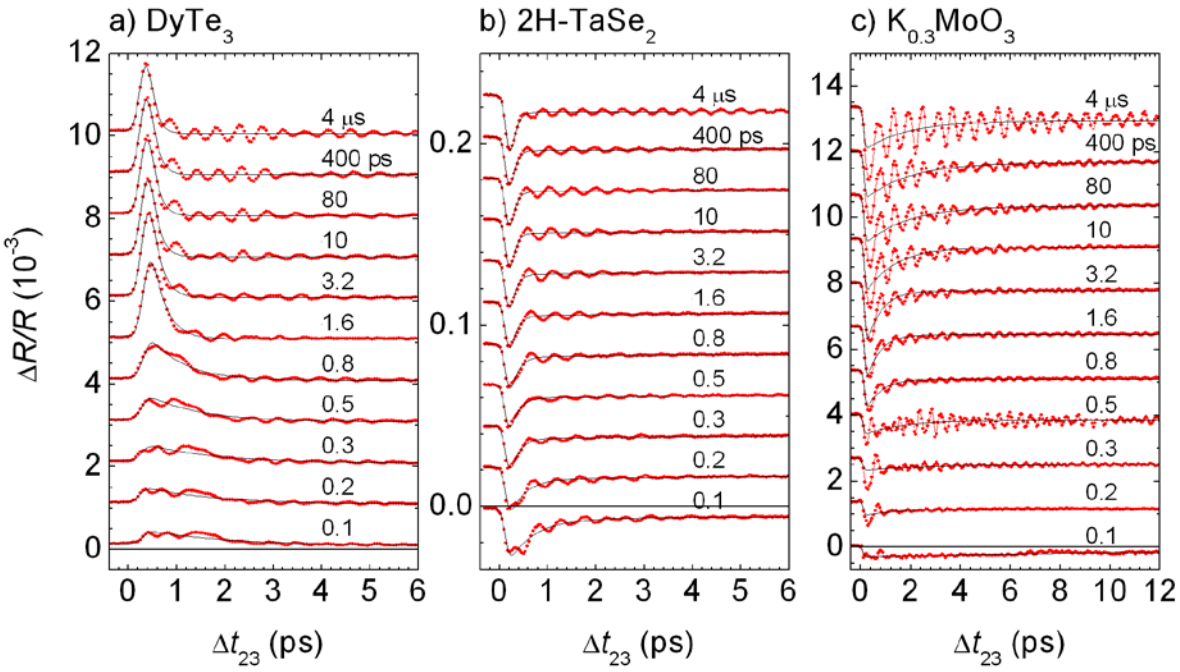

Figure 4: The raw reflectivity data recorded by the $P-p$ sequence for different time delays Δt_{12} in a) $DyTe_3$, b) 2H-$TaSe_2$ and c) $K_{0.3}MoO_3$. The fits are made to the data using a single exponential for a) and c), and a 2-exponential fit for b).

region around t_c, these have relatively small spectral weight, and give rise to low-frequency distortions of the spectral shape which are less intense. As a result the spectral shapes (intensities) are distorted vertically, with the largest intensity being at high frequency, near ω_0.

Comparison of $TbTe_3$ with $DyTe_3$, 2*H*-$TaSe_2$ and $K_{0.3}MoO_3$.

An important question of universality arises with regard to the observation of distinct timescales in the QP and collective mode dynamics in $TbTe_3$ summarised by the sequence: (1) subpicosecond gap recovery $\rightarrow$ (2) critical slowing down of the order parameter fluctuations through the transition ($t_c \sim 1-3$ ps) concurrent with the creation of multiple domains $\rightarrow$ (3) coherent topological defect annihilation (3-10 ps) . It is important to show that the observed concepts are universal beyond one specific material system.

$TbTe_3$ belongs to a universality class of Lorentz-invariant systems exhibiting second-order SBTs described by a complex order parameter, which also include the Higgs model and G-L model systems. In CDW systems the QP excitations are neutral, and the relaxation of the phase ϕ is slow compared to the relaxation of Δ, so the systems can be described by Eq. 1, irrespective

DOI: 10.1038/NPHYS1738

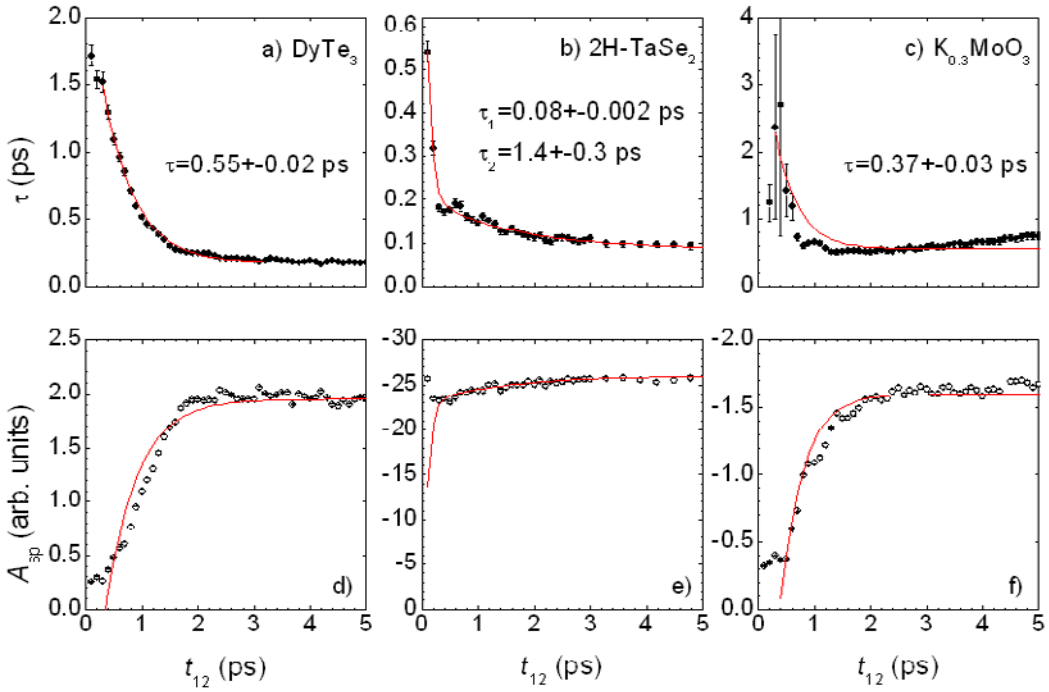

Figure 5: The gap recovery times τ_Δ from the decay of the QP lifetime τ_{QP} and amplitude A_{QP} are: a) $DyTe_3$: $\tau_\Delta = 0.55 \pm 0.02$ ps, b) $2H$-$TaSe_2$ (2-exponential) : $\tau_{\Delta 1} = 0.08 \pm 0.002$ ps, $\tau_{\Delta 2} = 1.4 \pm 0.3$ ps and c) $K_{0.3}MoO_3$: $\tau_\Delta = 0.37 \pm 0.03$ ps.

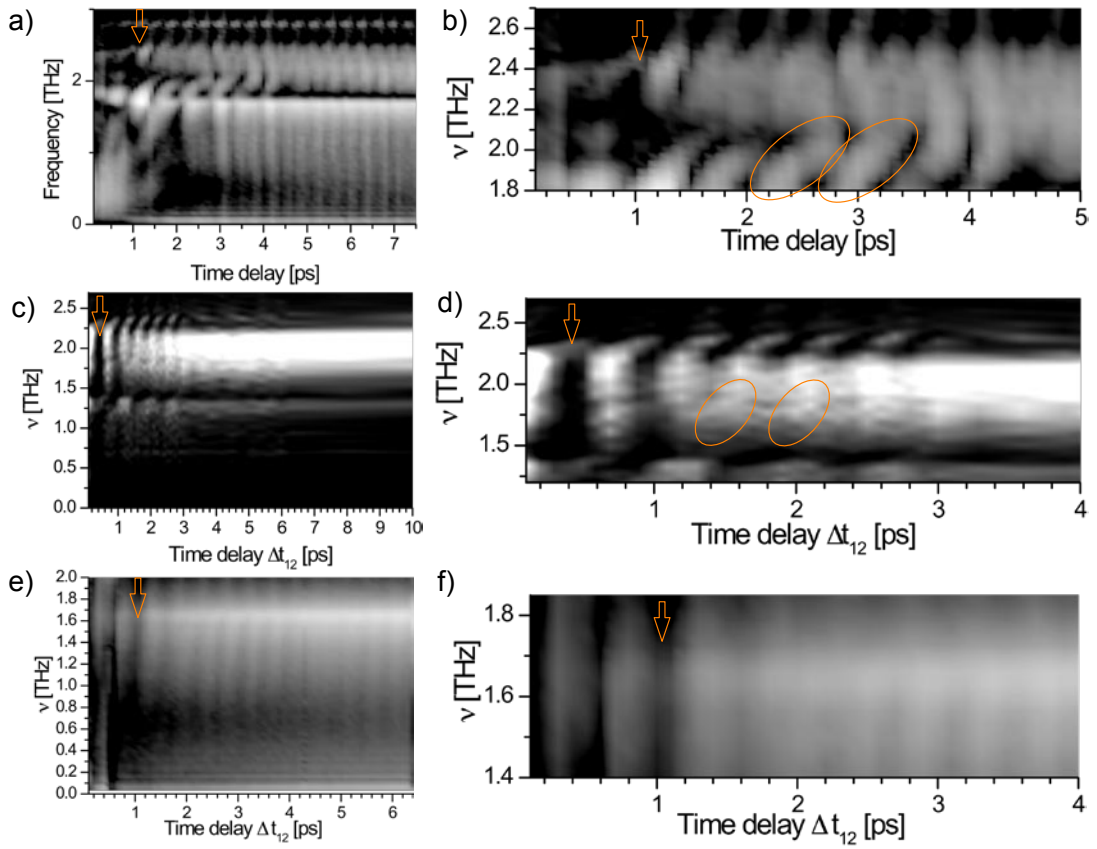

Figure 6: The power spectra of the oscillatory response for a) $DyTe_3$ full scale. The arrow shows the slowing down near t_s. b) An expanded section of the data for DyTe3 showing the diagonal distortions very clearly (circled). c) FFT data for $2H$-$TaSe_2$ thriough the transition. The arrow shows the slowing down near t_s. Note the slightly extended time between reflectivity maxima near t_s. d) An expanded view of the data for $2H$-$TaSe_2$ showing slight distotions between the vertical blobs. e) $K_{0.3}MoO_3$ data also obtained directly from data by FFTs. f) expanded view showing the critical slowing down behaviour near t_s, similar to the tellurides and the selenide. Diagonal distortions are not observed in this sample.

DOI: 10.1038/NPHYS1738

of the microscopic mechanism for the CDW formation. Topological defects will form if the broken-symmetry state allows the formation of multiple domains. Superconductors on the other hand, while displaying a second order transition and having a complex order parameter, have charged QPs, so the collective excitations are overdamped. Moreover, the relaxation of ϕ is faster than for Δ, so vortices are formed, rather than domains, as in the case of CDWs, so they do not belong to the same universality class.

Thus, to show that the observed evolution of events through the symmetry-breaking transition observed in $TbTe_3$ is independent of the microscopic nature of the system, we have performed identical experiments on three additional systems within the same universality class. The first is $DyTe_3$ which belongs to the same family of compounds as $TbTe_3$, and serves to confirm that the behaviour is general within one family of compounds. The two additional systems are 2*H*-$TaSe_2$ and $K_{0.3}MoO_3$ (blue bronze) which both have second-order SBTs and are very well characterised by many experimental techniques, including pump-probe experiments[9, 10]. Microscopically the materials are very different however. While 2*H*-$TaSe_2$ is a 2-dimensional layered system in which the transition is driven by Fermi surface nesting and the gap opening is only partial (so that it never becomes insulating), blue bronze is essentially a one-dimensional chain compound, with an archetypal Peierls instability occuring on the chains and displaying a metal-insulator transition near 180 K. In all cases some AM softening with temperature is observed (Fig. 6), which is $\sim$50 % in both 2*H*-$TaSe_2$ and $DyTe_3$ (which is almost as large as in $TbTe_3$), but is very weak (< 15%) in blue bronze, indicating a departure from the universality class of SBT defined by the tellurides and selenides. Thus for blue bronze we expect some departures from the predicted model behaviour, particularly related to softening of the AM and domain wall annihilation.

QP dynamics

In Figures 5 and 6 we show the evolution of the system through the SBT for the three materials. The raw data and a fit to the QP dynamics is shown in Fig. 5. The QP dynamics behaviour of $TbTe_3$ and $DyTe_3$ are almost identical. A single exponential fit can describe the dependence of τ_{QP} on Δt_{12} very well, and is consistent with the relaxation of the QP amplitude on a timescale given by the fit $\tau_{\tau_{QP}} \simeq \tau_{A_{QP}} \simeq 0.6$ ps for $DyTe_3$. There is some ambiguity of the QP amplitude recovery in 2*H*-$TaSe_2$, mainly because the QP amplitude is relatively small compared to the oscillatory component and it decays on a timescale which is comparable with the oscillation period of the AM (see raw data in Fig. 5b). A fit to the data suggests a two-exponential response, where the fast component recovery time is $\tau^{(1)}_{\tau_{QP}} \simeq \tau_{A_{QP}} \simeq 80$ fs, and the weaker slower component has $\tau^{(2)}_{\tau_{QP}} \simeq \tau_{A_{QP}} \simeq 1.4$ ps. In blue bronze the QP gap shows a recovery time of $\tau_{\tau_{QP}} \simeq \tau_{A_{QP}} \simeq 0.4$ ps. The universal feature of all four materials is that the QP excitations recover their broken-symmetry state gap within $\sim$1 ps or less.

Collective mode dynamics

In Fig. 6 we show the time-evolution of the FFT power spectra for the three compounds. The AM reflectivity modulations caused by the Ψ-field oscillations start within 1 ps of the D pulse in all three cases. They are clearly visible up to 6 ps, whereupon they start to die out. In blue bronze the behaviour through the SBT is less spectacular than in the other three materials because the intensity of the AM is weak in the first 2 ps.

Diagonal spectral features in the $\omega - t$ plots which can be attributed to Higgs waves are indicated by the arrows around 2-4 ps in $DyTe_3$ and around 1.6 ps in 2*H*-$TaSe_2$ albeit in the latter case, less clearly than in the tellurides. No diagonal distortions are observed in blue bronze, where all the distortions are vertical.

Further insight into the observed behaviour can be obtained from the G-L model calculation. Using the experimental parameters for three compounds (listed in the captions for Figures 5 and 7), and Eq. 2 of the main text, we computed the predicted reflectivity response which is shown in Fig. 7. The time-evolution of *A* as a function of depth and time is shown in Fig. 7 for each case in *z-t* plots. The model calculations correctly predict the critical fluctuations of the AM intensity and critical slowing down at the critical time of the transition t_c which is seen as the slightly longer period of fluctuations around 1.2 ps. From Fig. 7 f), we see that no Higgs waves on the surface are predicted for the blue bronze up to 10 ps, and indeed, none are observed (Fig. 7e)). For $DyTe_3$ and 2*H*-$TaSe_2$, (Fig. 7 a)-d)), the distortions arising from Ψ-waves emitted on annihilation of topological defects are predicted, and are discernible in Fig.6.

For illustration purposes we show the predicted behaviour for a much longer QP gap recovery time for 2*H*-$TaSe_2$ with quasiparticles lifetime of $\tau_{QP} = 1.4$ ps and 3 ps (shown in Fig. 8g) and h) respectively). We see that extending the QP gap recovery time leads to significantly different evolution of the Ψ field with time for longer QP times. As expected, these calculations bear no resemblance to any of the data in Fig. 7.

Considering the generality and simplicity of the model and the sensitivity of the solution to parameters arising from its strong non-linearity, the agreement with the data is quite remarkable. However, there are a few differences between the data and the calculations, which we will briefly note here. The intensity at short times, and particularly for times before the critical transition time is greater than observed. This is not surprising, considering the model takes no account of the changes in the dielectric constant at short times following the D pulse arising from the high-density electronic perturbation and ensuing screening by the photoexcited carriers. Also, the model does not take into account broadening of the AM near the transition described by α, nor does it take into account that, for $K_{0.3}MoO_3$ in particular, the softening of the AM near the transition is only partial [10].

We conclude that the distinct sequence of events through the SBT is common to all three materials $TbTe_3$, $DyTe_3$ 2*H*-$TaSe_2$ and $K_{0.3}MoO_3$ within the same universality class, regardless of their microscopic nature. Departures from the predicted behaviour appear to be associated with intrinsic departure from 2nd-order behaviour of the AM, particularly in $K_{0.3}MoO_3$.

DOI: 10.1038/NPHYS1738

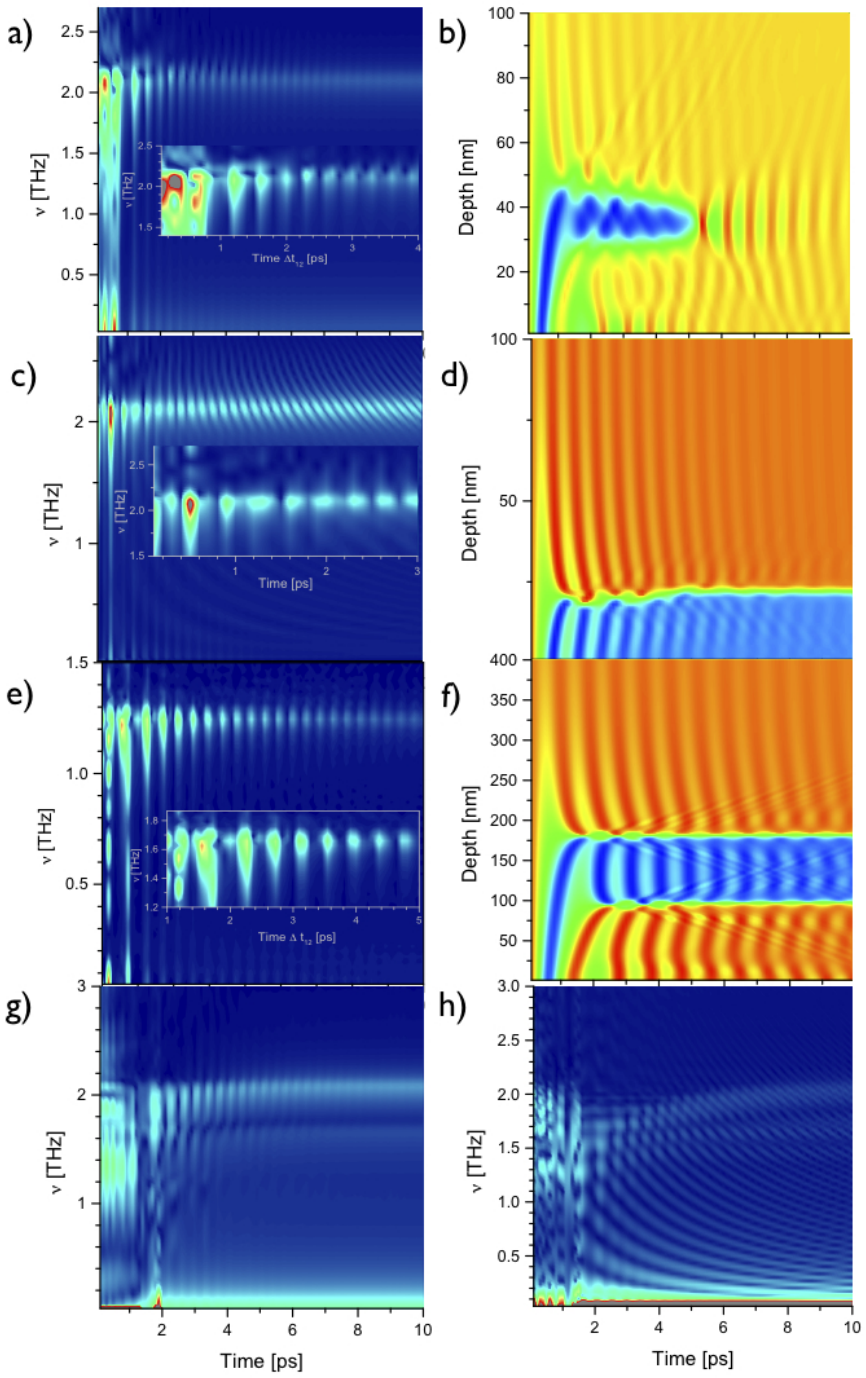

Figure 7: The predicted spectral response of the AM as a function of time delay Δt_{12} for a) $DyTe_3$ with model parameters: λ =20 nm, ξ = 1.3nm, ν =2.2 THz, $\Delta\nu$=0.2 THz, c) 2*H*-$TaSe_2$: with λ = 36nm[6], ξ=0.44 nm [11], ν = 2.18 THz, $\Delta\nu$ = 0.2 THz and e) $K_{0.3}MoO_3$: λ = 85 nm[4], ξ = 1.3 nm[12] and ν = 1.7 THz, $\Delta\nu$ = 0.1 THz. The domain structure calculated with the same parameters as a function of time is shown in b), d) and f) respectively for the three compounds. The colour scale spans from -1 (yellow) to +1 (dark blue). The domain walls are green, The QP gap recovery times used are given by the fits to the data in Fig. 4 for each of the three materials respectively. The two bottom panels show the model calculations for 2*H*-$TaSe_2$ with d) τ_{QP} =1.4 ps and e) τ_{QP} =3 ps (see text). The excitation parameter is typically $n = 1.5 \sim 2$.

Movie Legend.

In the supplement we present two movies ("Evolution of A(t) with gradient term.avi" and "Evolution of A(t) without gradient term.avi") which depict the numerical solution of the equation of motion (2) (given in the main text) with and without an additional gradient term $\frac{d^2A}{dx^2}$:

$$\frac{1}{\omega_0^2}\frac{d^2}{dt^2}A + \frac{\alpha}{\omega_0}\frac{d}{dt}A - \mu A + A^3 = 0 \tag{8}$$

and

$$\frac{1}{\omega_0^2}\frac{d^2}{dt^2}A + \frac{\alpha}{\omega_0}\frac{d}{dt}A + \frac{d^2A}{dz^2} - \mu A + A^3 = 0 \tag{9}$$

respectively. The gradient term is written in a dimensionless form, which means that the distance is measured in units of coherence length ξ. The parameters used are the same as used for generating the solutions in Fig.3 of the main text: AM frequency, $\nu_{AM} = 2.18$ THz and AM linewidth $\Delta\nu_{AM} = 0.2$ THz, A(0) = 1 and $\tau_{A_{QP}} = 0.65$ ps. The formation of two domain walls at depths of about 4 and 10-12 nm is clearly evident after 70 cycles (approximately 32 ps). When a gradient term is present, the propagation of a wave disturbance into the sample is seen.

Three panels are presented in the movies, depicting the amplitude A/A_0 at the surface (top), the depth dependence of the order parameter - represented by the colour - as a function of time (bottom left), and the depth dependence of A/A_0 (bottom right) as a function of time respectively. The domain annihilation event and emission (at around 4 s in the movie) of a Higgs waves proagating towards the surface and away from the surface are visible in the beginning of the movie describing the inhomogeneous solution (9).

Acknowledgments.

We wish to acknowledge Katica Biljakovic and Helmut Berger for $K_{0.3}MoO_3$ and $TaSe_2$ samples presented in the SOM.

References

[1] R.Yusupov et al., Phys. Rev. Lett., **101**, 246402 (2008).

[2] N. Ru et al., Phys. Rev., B **77**, 035114 (2008).

[3] P. Kusar et al., Phys. Rev. Lett., **101**, 227001 (2008).

[4] L. Degiorgi et al., Phys. Rev., B **44**, 7808 (1991).

DOI: 10.1038/NPHYS1738

[5] L. Degiorgi et al., unpublished data (2008).

[6] A R Beal , H P Hughes and W Y Liang, Journal of Physics C: Solid State Physics, **8**, 4236 (1975).

[7] V. L. Ginzburg, Sov. Phys. Usp. **5**, 649 (1963); V.L. Ginzburg A.P. Levanyuk, A.A. Sobianin, Uspekhi Fizicheskih Nauk, **130**, 615 (1980).

[8] H.J. Zeiger et al., Phys. Rev., B **45**, 768 (1992).

[9] J. Demsar et al., Phys. Rev., B **66**, 041101 (2002).

[10] J. Demsar et al., Phys. Rev. Lett., **83**, 800 (1999).

[11] R.A. Craven and S.F. Meyer, Phys. Rev., B **16**, 4583 (1977).

[12] For a review, see C. Schlenker, Low-Dimensional Electronic Properties of Molybdenum Bronzes and Oxides Kluwer Academic, Dordrecht p. 159, (1989), and J.-P. Pouget, ibid., p. 87.